Science of The Total Environment
Available online 12 October 2020, 142914
In Press, Journal Pre-proof
https://doi.org/10.1016/j.scitotenv.2020.142914

Comparative Study of Arsenic Removal by Iron-based Nanomaterials: Potential Candidates for Field Applications

Tonoy K. Das, Achintya N. Bezbaruah*

Nanoenvirology Research Group, Department of Civil and Environmental Engineering, North Dakota State University, Fargo, ND 58105, USA

HIGHLIGHTS

- Zero-valent Fe0 based nanomaterials removed arsenic better than the magnetite-based ones.
- Arsenic removal by nanohybrids was higher than their bare iron counterparts (nanoscale Fe^0 and magnetite)
- Graphene oxide-nano Fe0 was the most efficient nanohybrid for As(III) and As(V) removal (pH 3-9)
- Graphene oxide-nano Fe0 nanohybrid has potential for field applications for water treatment

Graphical Abstract

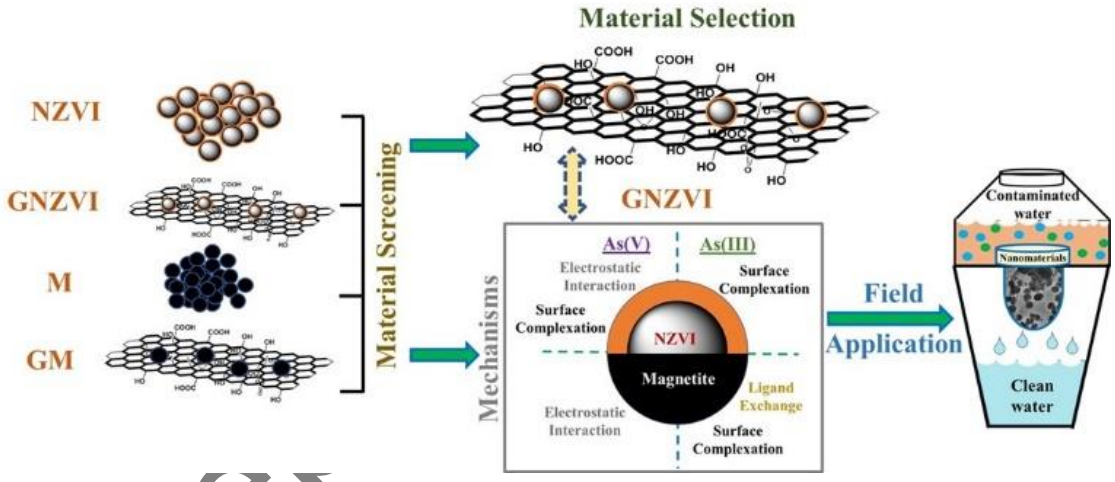

ABSTRACT: Graphene oxide supported magnetite (GM) and graphene oxide supported nanoscale zero-valent iron (GNZVI) nanohybrids were compared for arsenic removal at a wide pH range (3-9). While already published work reported high process efficiency for GM and GNZVI, they cannot be compared one-on-one given the non-identical experimental conditions. Each researcher team used different initial arsenic concentration, solution pH, and adsorbent dose. This study evaluated GM and GNZVI, bare magnetite (M), and bare nanoscale zero-valent iron (NZVI) for aqueous arsenic removal under similar experimental conditions. GNZVI worked more efficiently (>90%) in a wide pH range (3-9) for both As(III) and As(V), while GM was efficient (>90%) only at pH 3 for As(V) and As(III) removal was maximum of ~80% at pH 9. GNZVI also exhibited better aqueous dispersibility with a zeta potential of −21.02 mV compared to other adsorbents in this experiment. The arsenic removal based on normalized iron content indicated that the nanohybrids recorded improved arsenic removal compare to bare nanoparticles, and GNZVI worked the best. In NZVI-based nanomaterials (GNZVI and NZVI), electrostatic attraction played a limited role while surface complexation was dominant in removal of both the arsenic species. In case of M-based nanomaterials (GM and M), As(V) removal was controlled by electrostatic attraction while As(III) adsorption was ligand exchange and surface complexation. GNZVI has the potential for field application for drinking water arsenic removal.

Keywords: Arsenic; Adsorption; Graphene oxide; Magnetite; Nanoscale zero-valent iron

*Corresponding author. E-mail: a.bezbaruah@ndsu.edu ; Phone: 701-231-7461; Fax: 701-231-6185

1. Introduction

Arsenic is a naturally occurring carcinogenic metalloid presents in inorganic forms in groundwater and typically present in two oxidation states, As(III) or arsenite and As(V) or arsenate (ATSDR, 2007). Most of the arsenic present in groundwater is from geogenic sources (Amini et al., 2008; Podgorski and Berg, 2020) while the anthropogenic sources include some pesticides used in the past and industrial discharge (Murcott, 2012). World Health Organization (WHO) and the United States Environmental Protection Agency (USEPA) have set maximum contaminant level (MCL) of total inorganic arsenic in drinking water as 10 µg/L (USEPA, 2001; WHO, 2003). More than 200 million people in 50 countries are affected by groundwater arsenic contamination and the number is increasing rapidly (Murcott, 2012; Podgorski and Berg, 2020; WHO, 2018).

Adsorption has become a widely adapted technology for efficient removal of aqueous arsenic with the added advantages of ease of implementation and economic viability. While the selection of the right adsorbent is always challenging (Lata and Samadder, 2016), iron (Fe)-based metal-oxide nano-adsorbents were extensively studied for arsenic remediation in the last two decades. Nano-adsorbent have high specific surface area and good selectivity to remove both the inorganic arsenic species, and exhibited rapid reaction rates (Siddiqui et al., 2019; Wong et al., 2017). The major problem associated with these nanomaterials is their agglomeration that reduces their contaminant (arsenic) removal efficiency and, thus, limit their application. Synthesis of these nanomaterials on a suitable support medium reduces their agglomeration and significantly improves their arsenic removal efficiency (Liu et al., 2020) . Graphene oxide (GO) is one of the most promising support media extensively used by researchers (Sherlala et al., 2018; Yang et al., 2017). Graphene oxide is a 2D of carbon sheet with several functional groups (−COOH, −OH, C=O). The metal ions nucleate onto the GO surface and nanoparticles can be synthesized as well dispersed entities on the GO sheet. There are reported work on graphene oxide supported iron nanoparticles (aka graphene oxide iron nanohybrids) for arsenic removal. Most of the studies used graphene oxide magnetite (GM) nanohybrids as the adsorbent (Chandra et al., 2010; Hoan et al., 2016; Mishra and Ramaprabhu, 2012; Sheng et al., 2012; Yoon et al., 2016; Yoon et al., 2017). There are also report on graphene oxide supported nanoscale zero-valent (GNZVI) nanohybrids (Wang et al., 2014a). While each reported work had high process efficiency with >99% arsenic removal, they cannot be compared one-on-one given the non-identical experimental conditions. Each researcher team used different initial arsenic concentration (0.1-25 mg/L), solution pH (5.5-7.0), and adsorbent dose (0.1-0.4 g/L) (Table 1). Further, each of the reported nanohybrid had different iron content which might have significantly affected the arsenic removal efficiency. While both the materials (GM and GNZVI) appears to be efficient, there is no reported comparison of the nanohybrids under similar experimental conditions. Further, a comparative analysis of the mechanisms of arsenic removal by the two nanohybrids is imperative to better understand the materials and their potential applications for drinking water arsenic removal.

In this study, we evaluated GM and GNZVI, bare magnetite (M), and bare nanoscale zero-valent iron (NZVI) for aqueous arsenic removal under similar experimental conditions and amount of arsenic removal has been normalized with amount of iron present in each nanomaterial. The efficiency of arsenic removal by each nanomaterial has been evaluated and the removal mechanism(s) elucidated.

Table 1. Experimental conditions for arsenic removal by graphene oxide supported iron nanomaterials.

Adsorbents	pH*	Arsenic conc. (mg/L)	Adsorbent dose (g/L)	Source
Magnetite-rGO‡	7	3-7	0.2	(Chandra et al., 2010)
Magnetic-GO	6.5	25	0.4	(Sheng et al., 2012)
NZVI-Reduced GO	7	15	0.4	(Wang et al., 2014a)
GN-α-FeOOH Aerogel	8-9	5	0.05	(Andjelkovic et al., 2015)
β-FeOOH@GO-COOH	6.5	1	3	(Chen et al., 2015)
Fe_3O_4-GO	7	0.15-1	0.1	(Yoon et al., 2016)
Fe_3O_4-non-oxidative GO	7	1	0.1	(Yoon et al., 2017)
FeO_x GO	6.5	0.1	0.8	(Su et al., 2017)
Fe_2O_3 nanocubes-GO aerogel	5	5	0.5	(Yu et al., 2019)

*pH at which the experiment was conducted; ‡rGO: Reduced graphene oxide

2. Experimental methods

2.1. Materials and supplies

Graphene oxide (4 g/L in water, monolayer content >95%) was from Graphenea (Spain). Iron(II) chloride tetrahydrate ($FeCl_2 \cdot 4H_2O$, >98% pure), iron(III) chloride hexahydrate ($FeCl_3 \cdot 6H_2O$, 97-99%), ammonium hydroxide (NH_4OH, 30%), ferrous sulfate ($FeSO_4 \cdot 7H_2O$, >99.5%), sodium borohydride ($NaBH_4$, >97%), and other chemicals from VWR (USA). All chemicals were reagent grade and used as received unless otherwise specified. A 1000 mg/L standard stock solution (Environmental Express, USA) was used to prepare various As(III) and As(V) solutions by diluting with deoxygenated deionized (DDI) water.

2.2. Material synthesis

Preparation of GM and M: Graphene oxide-magnetite (GM) nanohybrids were prepared as per Yoon et al. (2016). Briefly, 200 mg GO (i.e., 50 mL of 4 mg/L GO solution received from the manufacturer) was mixed within 150 mL DDI water in a 250 mL glass bottle and ultra-sonicated (FS30, Fisher Scientific) for 1 h to disperse the GO. Then the GO solution was transferred into a 300 mL round-bottom reaction flask. The reaction flask was placed in an oil bath connected to a temperature controller assembly (ACE Glass Inc., USA). The oil bath assembly along with the reaction flask was placed on a magnetic stirrer and continuously stirred. The content in the reaction flask was purged with nitrogen gas (N_2) for 30 min to deoxygenate the GO solution. Separately, two solutions of $FeCl_2 \cdot 4H_2O$ (0.4 g) in 0.5 M HCl (10 mL) and $FeCl_3 \bullet 6H_2O$ (1.04 g) in DDI water (20 mL) were prepared in two 50 mL centrifuge tubes, and then combined together to get an iron solution with a $FeCl_2$:$FeCl_3$ molarity ratio of ~2:1. The mixed iron solution was added slowly to the GO solution in the reaction flask (with continued N_2 purging and stirring). As the pH of the solution was adjusted to 10 by dropwise addition of 30% NH_4OH, the solution became blackish in color. To facilitate nanoparticle formation, the solution in the reaction flask was cooked for 2 h at 75-80 °C with continued N_2 purging and stirring (the open top of the reaction flask was wrapped with an aluminum foil to reduced evaporation losses). The black-colored solution was then transferred to two 50 mL centrifuge tubes and centrifuged at 3000 rpm for 5 min. The nanomaterials precipitated and the supernatant was decanted. The nanoparticles were then washed two times each first with DDI water and then with ethanol (analytical grade) to remove unreacted chemicals. Washing was done by filling up the tubes with DDI water or ethanol and centrifuging them at 3000 rpm for 5 min and then decanting out most of the liquid. The washed nanomaterials were dried at 40 °C under nitrogen environment in a vacuum oven (VWR, USA) for 40 h. The dried nanomaterials (GM nanohybrids here) were ground into powder using an agate pestle and mortar. The powdered nanohybrid was stored in 20 mL glass vials with the headspace flushed with N_2 gas. For bare magnetite (M)

preparation, the same procedure was used without the addition of GO.

Preparation of GNZVI and NZVI: Graphene oxide supported nanoscale zero-valent (GNZVI) nanohybrids were synthesized after others (Wang et al., 2014a) with modifications to optimize the pH and borohydride dosing. GO (62.5 mL of 4 g/L GO solution received from the manufacturer = 250 mg) in DDI water (62.5 mL) was exfoliated by ultra-sonication. The GO solution was then transferred into a round-bottom reaction flask (300 mL) and placed on a temperature-controlled oil bath put on a magnetic stirrer for continuous stirring. To deoxygenate the GO solution, the content in the reaction flask was purged with N_2 gas for 30 min. On the side, a $FeSO_4 \cdot 7H_2O$ solution (2.25 g in 50 mL DDI water) was prepared in a volumetric flask (50 mL) and poured into the GO solution very slowly, and the new solution was continuous stirred and purged with N_2 gas for ~30 min. By dropwise addition of 1 M NaOH or HCl, the pH of the GO-Fe solution was adjusted to 6.1 before an aqueous solution of $NaBH_4$ (0.99 g in 30 mL of DDI) was added dropwise to the reaction flask with continuous stirring and N_2 purging on. When the solution turned blackish, the solution temperature was raised to and maintained at 60 ºC for 4 h for the reaction to complete (a black colored product was formed). The black-colored product was transferred to 50 mL centrifuge tubes for centrifugation (3000 rpm). After centrifugation, the supernatant was decanted, and the black product was washed with amount of DDI water and then with ethanol (two times each). The resulting black solids were vacuum-dried (40 h, 40 ºC, and under N_2 environment). The dried nanomaterials were GNZVI nanohybrids. The nanohybrids were ground using an agate pestle and mortar, and the powers were stored in a 20 mL glass bottle with the headspace flushed with N_2 gas. For bare NZVI synthesis, the same procedure was used but without the addition of GO as per our previously published method (Bezbaruah et al., 2013).

2.3. Characterization

Scanning electron microscopy (SEM): The GM, M, GNZVI, and NZVI samples were characterized with a JEOL JSM-7600F field emission scanning electron microscope (JEOL USA Inc., Peabody, Massachusetts) operated at 2 kV. The samples of nanomaterials were placed on carbon adhesive tabs (Ted Pella, Redding, California USA) attached to aluminum mounts and the excess material blown off with a stream of dry N_2 gas. Images were obtained with a JEOL JSM-7600F. Energy dispersive spectroscopy (EDS) data were obtained using an UltraDry silicon drift X-ray detector and NSS-212e NORAN system 7 X-ray microanalysis system (Thermo Fisher Scientific, Madison, Wisconsin).

Transmission electron microscopy (TEM): For TEM analysis, the specific powdered nanomaterial was placed in 100% ethanol and sonicated. A drop of the suspension was placed on a lacey-carbon support film on a 300-mesh copper TEM grid (Ted Pella, Redding, California USA) for 30 sec, then wicked off with a filter paper and allowed to air dry. High-Resolution TEM data were obtained using a JEOL JEM-2100 LaB_6 transmission electron microscope (JEOL USA, Peabody, Massachusetts) ran at 200 kV.

X-ray photoelectron spectroscopy (XPS): The XPS analyses (K-Alpha XPS, ThermoFisher Scientific) were done for the nanomaterials. Powdered samples were packed into small wells of 3 mm diameter and 3 mm deep. High-resolution scans were made for Fe2p, As3d, C1s, and O1s. The settings were: Pass energy = 50 eV, Dwell Time = 50 ms, spot size = 400 µm, Step size = 0.1 eV for a total of 10 scans per sample. The flood gun was also turned on to prevent charging the samples. Peak fitting was accomplished with Avantage XPS program.

Zeta potential (ζ): Zeta potential was measured with Zetasizer Nano ZS (Malvern, UK) at pH 7.5. The pH was adjusted to 7.5 by dropwise addition of 0.1 N HCl/NaOH after putting nanomaterial in the DDI water.

Point-of-zero-charge (PZC): PZC values were determined for the four materials used. We prepared a 0.01 M NaCl solution and adjusted the pH to the required value (pH 2-12) using 0.1 M NaOH or HCl. A measured amount (20 mg) of the nanomaterials was dispersed in 20 mL NaCl solution with different initial pH (Balistrieri and Murray, 1981; Lataye et al., 2006). The initial (0 h) and the final (48 h) pH values were recorded, and the PZC for each material was calculated by plotting initial pH vs. change in pH (dpH = Initial pH − Final pH). PZC of the adsorbent is the pH

when surface change on the material is zero and represented by the point where the plot (initial pH vs dpH) intersects the X-axis.

2.4. Experimental design

The primary objective of this study was to compare the four selected nanomaterials namely Graphene oxide-magnetite nanohybrid (GM), graphene oxide-nanoscale zero-valent iron nanohybrid (GNZVI), bare nano magnetite (M), and bare nanoscale zero-valent iron (NZVI), and screen out which one of these materials work most efficiently for the removal of aqueous As(III) and As(V). As(III) and As(V) were tested in separate batches. Amber glass vials (40 mL) fitted with a plastic cap and silicon septum were used as batch reactors. Each batch reactor contained 30 mL of arsenic solution (5 mg/L) with 10 mg of adsorbents (~333 mg/L). The reactors were rotated in a custom-made end-over-end shaker (28 rpm) for 24 h at room temperature (22±2 ºC). After 24 h, the reactors were withdrawn from the shaker and the content was filtered using 0.22 µm nylon housing single-use syringe filters (VWR, USA). The filtrate was acidified with concentrated HNO_3 (15.8 N) and kept in refrigerator for later analysis. The arsenic in the filtrate was measured using a graphite furnace-atomic absorption spectrophotometer (GF-AAS, Perkin Elmer AAS 900H). The percent removal efficiency of adsorbents was calculated as percent arsenic removal ($\eta = (C_0 - C_e)/ C_0 * 100\%$ where C_0 is the initial and C_e is the equilibrium arsenic concentration).

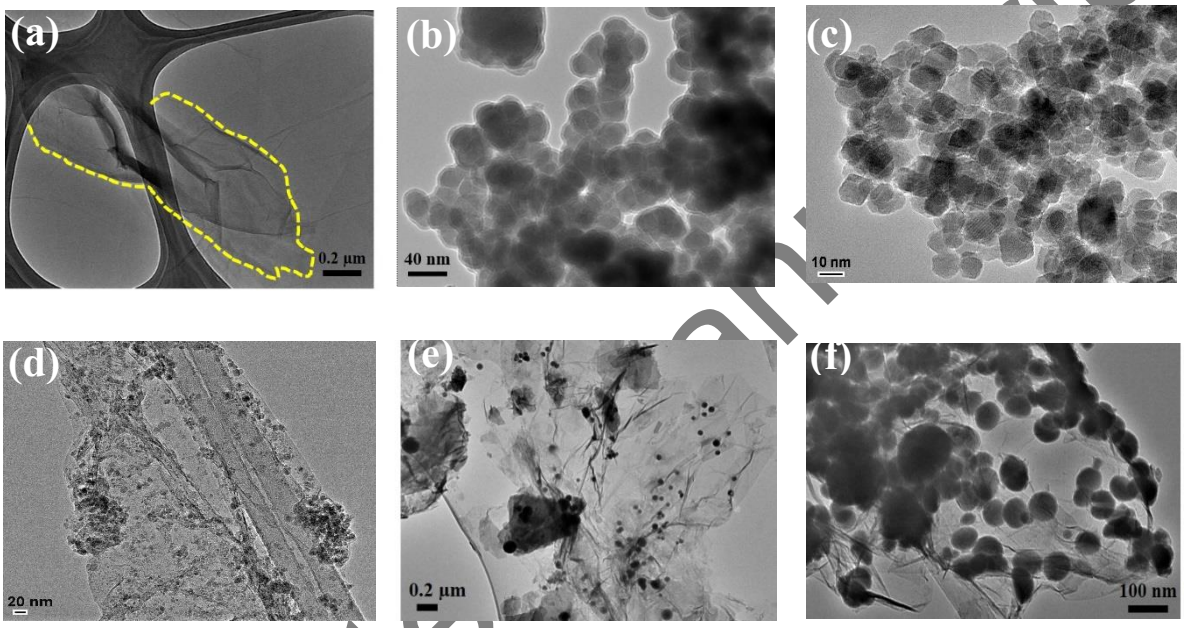

Fig. 1. TEM micrographs of: (a) GO sheet (dotted outline), (b) NZVI, (c) M, (d) GM, (e) GNZVI, and (f) HRTEM of GNZVI (core-shell structured NZVI particles trapped between GO layers).

The nano-based adsorbents (333 mg/L) used in our experiments did not contain the same amount of iron. While GNZVI and GM contained GO, their bare counterparts NZVI and M did not, and the amount of iron in each material was different. So, 333 mg of each material used in the batch studies did not contain the same amount iron (Fe). Therefore, we determined the total iron content in the nanomaterials for the comparison of their removal efficiencies based on the mass of iron (Fe) present. Here, 50 mg of an adsorbent was digested with 15 mL of 7M HCl by first shaking (250 rpm) for 2 h in a 50 mL test tube and then keeping it in a water bath for 1 h at 80 ºC. The digested sample was filtered using a membrane filter (0.22 µm, VWR, USA) and the iron concentration in the filtrate was measured using Flame AAS (Perkin Elmer AAS 900H). The amount of arsenic adsorbed (q_e, mg/g) as per unit

iron mass was determined as $q_e = (C_0 - C_e)$ *V/m, where V is the volume of solution (L), and m is the mass iron in the adsorbent (g).

2.5. Quality control and statistical analysis

All experiments were conducted in triplicates and the average values are reported here along with the standard deviations. All data analysis and graphical representation was done in OriginLab (OriginPro) software. ANOVA analysis was done to determine statistically significant differences in data sets and Tukey's pairwise comparison was used to identify the data that were significantly different.

3. Results and discussion

3.1. Material characterization

The four adsorbents and bare GO were examined under TEM. The GO sheets appeared as crumbled in nature and paper-like structures with irregular shape (Fig. 1a). The bare nanoparticles

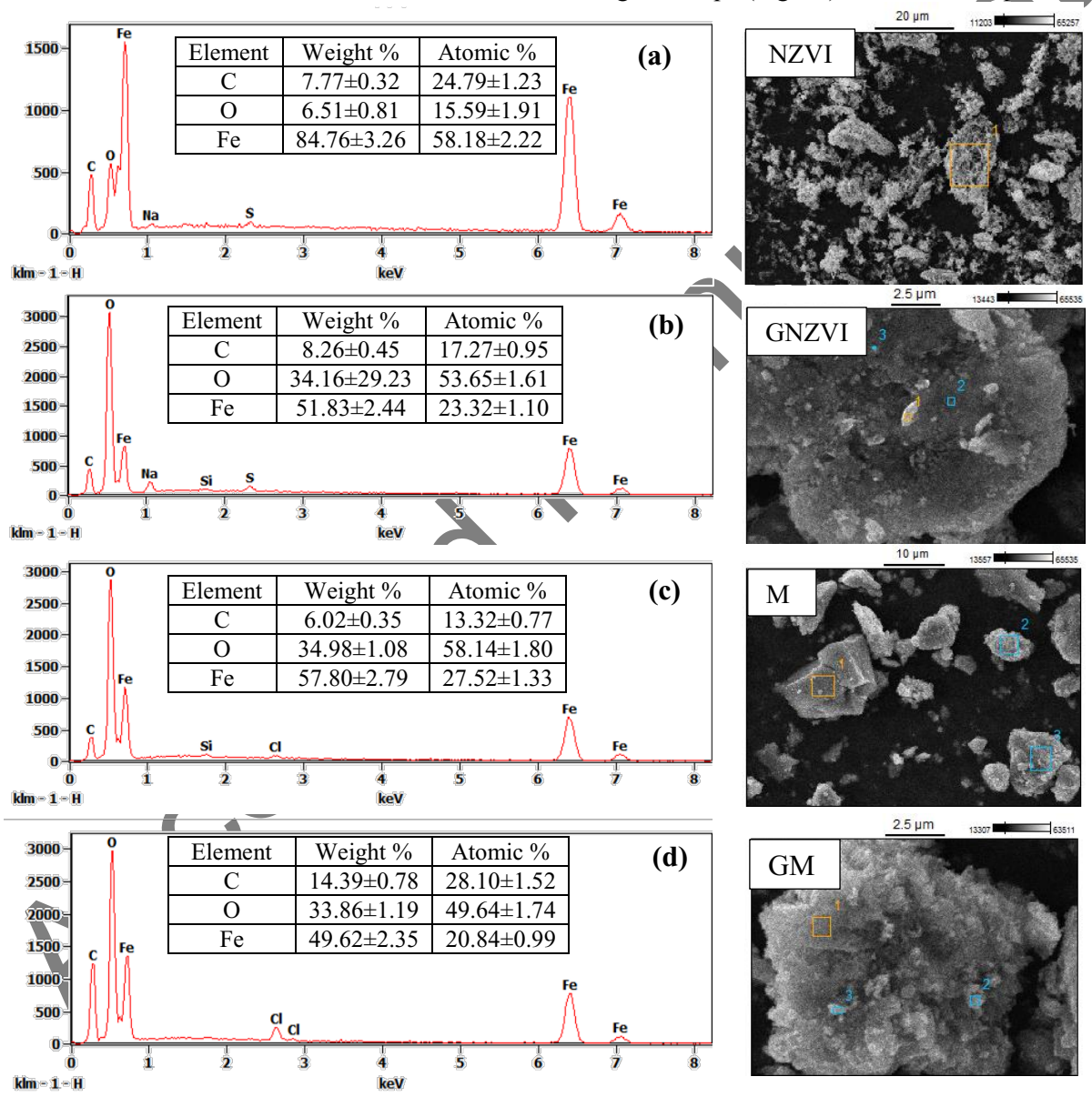

Fig. 2. SEM-EDS of fresh (a) NZVI, (b) GNZVI (c) M (d) GM.

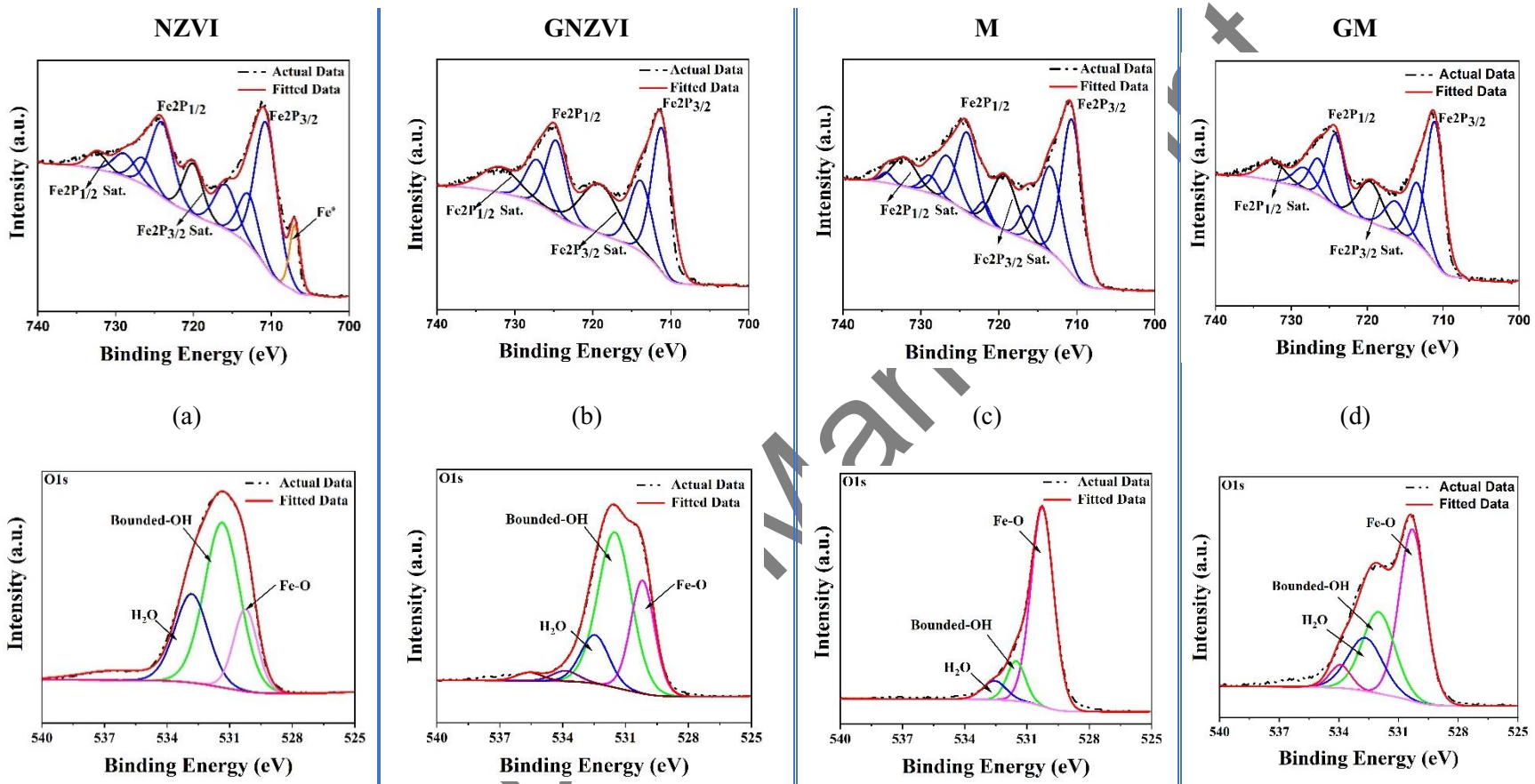

Fig. 3. High resolution-XPS spectrum of Fe2P and O1s obtained from (a) NZVI (b) GNZVI (c) M (d) GM

(NZVI and M) exhibited spherical morphology and were agglomerated (Fig. 1b-c). The particle size of NZVI ranged between 12.3 and 70.5 nm (n = 20) and for M, it was 6.7 to 20.9 nm (n = 20). On the nanohybrids, the iron nanoparticles (NZVI or M) were well dispersed on the GO surface (Fig. 1d-f). The particles were not only deposited on the surface of GO, but some of the particles were also sandwiched inside the GO layers. The particle size of NZVI deposited on GO in GNZVI (Fig. 1e-f) was 18.1-95.6 nm (n = 31), and for GM (Fig. 1d), it was 5.5-12.5 nm (n = 22). Similar morphologies of nanohybrids were reported by others (Das et al., 2020; Wang et al., 2014a; Yoon et al., 2016). The SEM-EDS data for bare NZVI (Fig. 2a) indicated the presence of 84.76% Fe and low oxygen (6.51% O) indicating the presence of elemental Fe (Fe^0) in the NZVI particle with a thin oxide layer (core-shell structure). The presence of a very thin (2-4 nm) oxide layer on NZVI was reported by others as well (Krajangpan et al., 2012; Martin et al., 2008).

In bare M (Fig. 2c), the oxygen content was found to be high (34.98%) and the Fe content (57.80%) was relatively low indicating the formation of iron oxides. Once nanoparticles were deposited on the GO surface (in both GNZVI and GM), the total oxygen (O) content increased and carbon (C) showed up prominently (Fig. 2b-d) as O and C also came from the GO sheets and the functional groups present.

XPS analyses of fresh NZVI (Fig. 3a) show the presence of both Fe2p and O1s spectra suggesting that the surface layer had both Fe_2O_3 and FeOOH. The Fe2p spectrum represents characteristic peak for Fe ($2p_{3/2}$ and $2p_{1/2}$) and the shake-up satellite peaks indicate the existence of Fe(II) and Fe(III). A small peak for metallic iron (Fe^0) was also observed. The existence of a large fraction of iron oxides and a relatively small amount of elemental iron (Fe^0) confirms that the NZVI surface was largely made up of iron oxides. This is in conformity with core-shell structure of NZVI which is also observed in our HRTEM micrographs (Fig. 1b) and reported by others (Tucek et al., 2017; Martin et al., 2008). The Fe2P peaks of GNZVI (Fig. 3b) look similar to those of NZVI sample except that there is no Fe^0 peak. The lack of Fe^0 peak may be due to the thin metal oxide layer and/or GO layer between which nanoparticles were trapped as that might have prevented the XPS beam from reaching the Fe^0 core. However, the core-shell structure is apparent in the HRTEM micrographs of GNZVI (Fig. 1f). Both Fe^{2+} and Fe^{3+} are present in the GNZVI with the peak positions suggesting the presence of both Fe_2O_3 and FeOOH with the O1s peaks indicating a higher concentration (~53.3%) of bounded OH. In M (Fig. 3c), the $Fe2p_{3/2}$ and $Fe2p_{1/2}$ peaks confirm that both Fe^{2+} and Fe^{3+} are present, and Fe_3O_4 formation is confirmed from the characteristic peaks of $Fe2p_{3/2}$ at ~710.63 eV and ~724.08 eV and the peak of O1s at ~730.27 eV (Chandra et al., 2010; Yoon et al., 2016). The satellite peak situated at ~719.32 eV is the characteristic peak of Fe^{3+} in γ-Fe_2O_3 (Grosvenor et al., 2004) suggesting that the M (Fe_3O_4) nanoparticles were partly transformed to maghemite ($Fe_3O_4 + 2H^+ \rightarrow \gamma\text{-}Fe_2O_3 + Fe^{2+} + H_2O$). The O1s peaks confirm the dominance (~79%) of Fe-O. The peaks from GM (Fig. 3d) are similar to those from the M indicating the presence of a majority of Fe_3O_4. The XPS analyses confirmed the successful synthesis of the four nanomaterials.

3.2. Dispersion behavior

Zeta potential (ζ) is the interfacial potential difference between charged material surface and the counter ions in the surrounding diffuse layer and is a measure of dispersibility of nanomaterials in aqueous phase. Particles $\zeta > |\pm 25|$ mV make a stable suspension (ISO, 2000). The ζ values were measured for NZVI, M, GNZVI, and GM as well for bare GO in DI water (Table 2). GO with a high negative ζ (-41.76 ± 2.27 mV) remained well disperse (stable) in water. The high ζ values of GO can be attributed to the presence of many functional groups (−COOH,−OH, C−O−C, C=O) on the GO surface which led to the negative surface charge upon ionization in water (Gao, 2015). The bare nanoparticles (NZVI and M) showed very low positive ζ (13.74 ± 0.59 mV for NZVI and 10.18 ± 0.72 mV for M), and they agglomerated and settled down easily. Both the nanohybrids recorded higher ζ (GNZVI: -21.02 ± 0.77 mV and GM: -17.44 ± 0.85 mV) than its bare counter parts leading to stable dispersions. There was, however, a reduction of ζ values in the nanohybrids compared to bare GO possibly due to the decrease in functional group and positive charge of iron nanoparticles during metal ion nucleation and

Table 2. Zeta potential (ζ) at pH 7.5 and point of zero charge (PZC) the nanomaterials used in this study.

Material	PZC	Mean ζ (mV)
GO	NM	-41.76±2.27
NZVI	8.4	13.74±0.59
M	4.3	10.18±0.72
GNZVI	8.05	-21.02±0.77
GM	4.8	-17.44±0.85

NM: Not measured as GO showed no significant arsenic adsorption; *pH of the test solution during ζ measurements

because of the presence positive changes on the nanoparticles surface. As the metal ions got attached to the functional groups on the GO surface, some negative charges present on the GO got neutralized leading to the decrease in net ζ values but the values were still relatively high compared to bare particles (NZVI and M) to achieve much better stable dispersions.

Solution pH plays an important role in the arsenic removal process by iron-based materials (Wang et al., 2014b; Yoon et al., 2016). The PZC (pH dependent surface charge properties) values for the four adsorbents varied from 4.3 to 8.4 (Table 2) with the nanohybrids having the PZC values as 8.05 (GNZVI) and 4.8 (GM). The surface of the adsorbent is positively charged at pH below the PZC and negatively charged at pH above PZC, and that may major play a role in arsenic removal. The speciation of the arsenic oxyanions is also

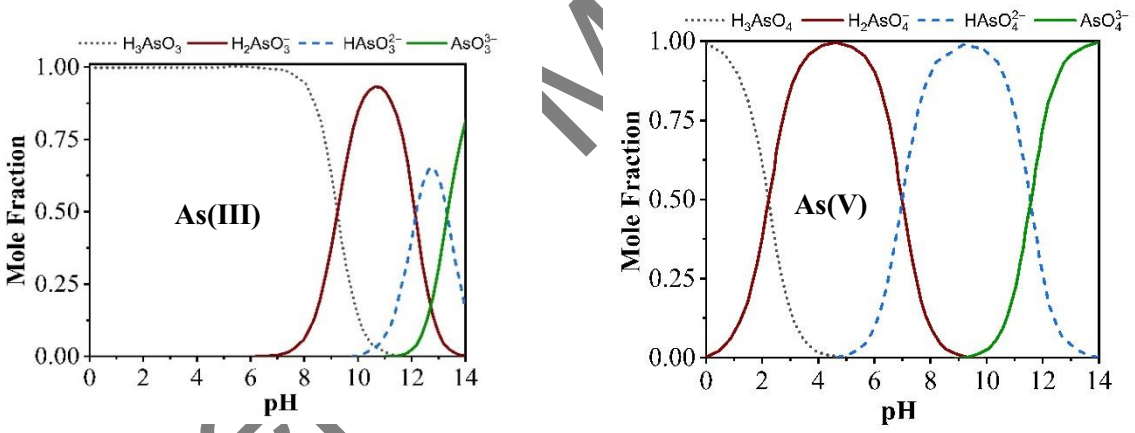

Fig. 3. Speciation of aqueous arsenic at different pH (modified after Ben Issa et al., 2011)

changed with solution pH (Fig. 4). The dominant As(V) species present in aqueous solution are H_3AsO_4 (at pH<2.2), $H_2AsO_4^-$ (pH 2.2-6.9), $HAsO_4^{2-}$ (pH 6.9-11.5), and AsO_4^{3-} (pH > 11.5). On the other hand, As(III) species are present in aqueous media as neutral H_3AsO_3 (pH<9.2) and $H_2AsO_3^-$ (pH>9.3).

3.4. Arsenic removal

3.4.1. *As(III):* GNZVI and NZVI removed >99% As(III) (initial concentration, C_0 = 5 mg/L) at pH 3-9 (Fig. 5a). There was no significant difference in As(III) removal by the two nanomaterials (Two-way ANOVA, p = 0.05). The PZC values for both GNZVI and NZVI were > 8, yet the removal efficiency did not change over the wide pH range and that leads us to think that surface complexation might have played a major role in As(III) removal here.

For GM and M, there was an increase in As(III) removal efficiency with the increase in pH (Fig. 5a). Others (Chandra et al., 2010; Yoon et al., 2016) also reported similar observations. Above

the PZC, M (PZC = 4.3) and GM (4.8) become negatively charged while As(III) remains mostly neutral (no charge) at pH < 9.2 and without any dominant repulsive force between the adsorbent and As(III), arsenic is still adsorbed onto GM and M. Here, As (III) removal is achieved potentially via surface complexation and ligand exchange. Others (Morin et al., 2009) suggested that: (1) There are some vacant tetrahedral site on the magnetite surface (111), and As (III) can fit into those sites by forming stable ^{3}C tridentate, hexanuclear, corner-sharing surface complexes, and (2) a portion of As(III) precipitates as amorphous Fe-As complex on the surface of magnetite. In ligand exchange process, the surface hydroxyl groups are replaced by arsenite ion. The amount of surface hydroxyl groups increases with the increase pH (Su et al., 2017) and thus contributing towards increased As(III) removal at higher pH (Kumar and Jiang, 2017).

3.4.2. *As(V):* Both the NZVI based adsorbents, GNZVI and NZVI recorded 87-98 % of As(V) removal (C_0 = 5 mg/L) over a wide pH range (3-9) (Fig. 5b). The maximum As(V) removal efficiency (>98%) was achieved at pH 5-7 (Fig. 5b). In our experimental pH range As(V) is present as negatively charged oxyanions ($H_2AsO_4^-$ and $HAsO_4^{2-}$). Now, the surfaces of GNZVI (PZC 8.05) and NZVI (PZC 8.4) are positively charged when the solution pH is below there PZC value. The negatively charged arsenic ions can be easily adsorbed onto the positively charged material surface through the columbic attraction. The material surfaces remain positive surface due to protonation of surface hydroxyls present on the iron oxide shell of NZVI. With the increase in solution pH, the amount of positive surface charges would decrease, and the arsenic adsorption onto the surface should decrease. However, there was no significant reduction in As(V) removal (Two-way ANOVA, p = 0.05) at pH 3 through 9 and that indicates that electrostatic attraction is not the only driving force for As(V) removal by GNZVI and NZVI. Similar findings were also reported by others literature (Wang et al., 2014a; Wu et al., 2017).

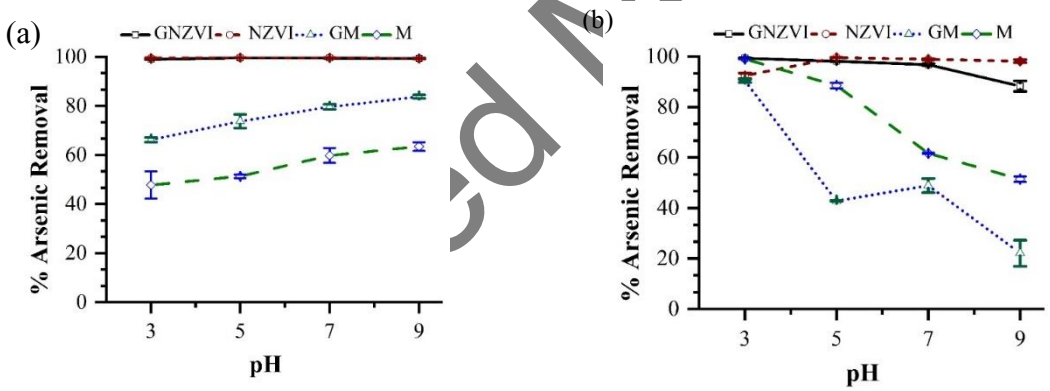

Fig. 5. Arsenic removal at different pH by four nanomaterial: (a) As(III); note: plots for GNZVI and are overlapped as both have similar removal efficiencies; (b) As(V). Initial arsenic concentration = 5 mg/L, Adsorbent dose = 333 mg/L Reaction Time = 24 h. The vertical errors bars represent standard deviations. The data points joined by straight lines for ease of reading only and the do not represent trendlines.

The NZVI is highly reactive, the Fe^0 reacts with water to continuously form iron oxide corrosion products such as FeOOH, Fe_3O_4, and Fe_2O_3. As(V) reacts with freshly generated iron oxide via inner sphere surface complexation forming monodentate or bidentate complexes. While electrostatic forces play a role at pH below the PZC, arsenic interactions with iron corrosion products on the surface of the NZVI particles apparently play the important roles in the As(V) removal process at all pH values. While the surface positive charge decreases with the increase in pH and electrostatic As(V) adsorption goes down, the increased As(V) complexations onto surface corrosion products offset the reduction, and so a consistent high

arsenic removal over a wide pH range was observed in this study.

For GM and M, As(V) removal decreased as the pH increased (Fig. 5b). At pH 3, ~90% As(V) removal was achieved with GM and ~99% with M, and the removal decreased when pH was raised to 9 (only 22% removal by GM and 51% by M). Given that GM and M was relatively more effective at pH below their PZC (4.8 for GM and 4.3 for M), we can infer that electrostatic force was dominant in arsenic removal. At pH higher than PZC, there was a net decrease in positive surface charge on the nanomaterials and so negatively charged As(V) ions were not attracted. Further, at high pH, the competition between As(V) species ($H_2AsO_4^-$ or $HAsO_4^{2-}$) and OH^- ions for adsorption sites might have affected arsenic removal.

Table 3. Arsenic removal by the nanomaterials used in this study.

Material	Particle Size (nm)$^+$	pH*	Fe content mg/g	As Loading mg/g**	
				As(III)	As(V)
NZVI	12.3-70.5	3-9	0.59	26	32-36
M	6.7-20.9	As(III): 9 As(V): 3	0.66	11.1-14.7	16.1-30.5
GNZVI$^+$	18.1-90.5	3-9	0.43	36	43-49
GM$^+$	5.5-12.5	As(III): 9 As(V): 3	0.44	23-29	10.4-41.7

*pH at which >90% arsenic removal was achieved; **mg of As per g of Fe; $^+$Size of the NZVI or M particles deposited on the graphene sheet

3.4.3. Comparison of the nanohybrids:

Comparison between nanohybrids and nanoparticles: In our study, we used 333 mg/L of each adsorbent (GNZVI, NZVI, GM, and, M) without normalizing for the amount of Fe present. We determined the Fe content in the four adsorbents (Table 3) to calculate the amount of arsenic adsorbed per unit mass of Fe (Fig. 6a-b). The Fe mass normalized data indicate significant improvement in arsenic removal when iron nanoparticles (NZVI, M) are decorated on GO surface (Table 3, Fig. 6a-b). GNZVI removed 10 mg more As(III) per g of material across all pH (3-9) compared to NZVI, and for As(V), the improvement was 11-13 mg at different pH values. As(III) removal by GM improved by 11.9-14.3 mg compared to that by M, and the improvement was ~11.2 mg for As(V). Higher arsenic removal by the nanohybrids (GZVI and GM) was achieved possibly because of their effective dispersion (reduced agglomeration) in aqueous media which ensured improved interaction with the arsenic species.

Comparison between GNZVI and GM nanohybrids: Comparison of arsenic removal by GNZVI and GM indicates that GNZVI is significantly ($p = 0.05$) more efficient than GM. Analysis based on normalized Fe content (Table 3, Fig. 6a-b), GNZVI removed ~36 mg As(III)/g of Fe and 43-49 mg As(V)/g, while GM removed 23-29 mg As(III)/g and 10-42 mg As(V)/g.

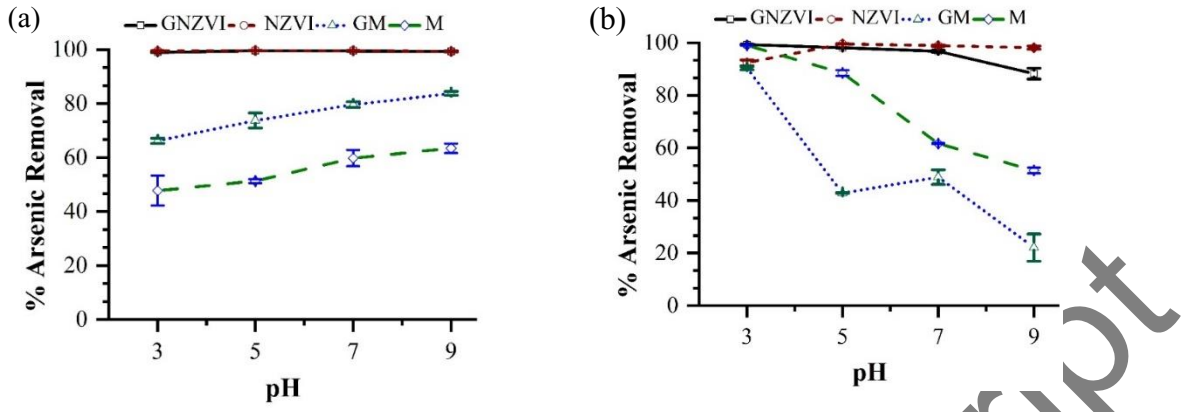

Fig. 6. Efficacy of arsenic removal based on iron mass present in the four nanomaterials: (a) As(III) and (b) As(V)

It is known that iron oxides are responsible for arsenic adsorption (iron oxide + arsenic → arsenic-iron complex) onto iron nanoparticles (Bezbaruah et al., 2013; Kanel et al., 2006; Rashid et al., 2020; Tucek et al., 2017; Wang et al., 2014b). Higher removal by the NZVI-based material is achieved possibly because of the continuous corrosion to leading to fresh iron oxide formation on the nanoparticle surface (shell).

3.4.4. Post arsenic sorption XPS analyses of the nanohybrids:

The nanohybrids (GNZVI and GM) so far worked better than their bare counterparts (NZVI and M), and so XPS spectra were collected after the graphene oxide-iron (GNZVI and GM) sorbed arsenic (As(V)/As(III)). The As(V)-sorbed GNZVI show a strong peak at ~ 45.57 eV (Fig. 7a, As 3d spectra) which is the characteristic peak for As(V). This indicate that As(V) was sorbed onto the surface of GNZVI and the oxidation state remained unchanged. In the case of As(III)-sorbed GNZVI (Fig. 7b, As3d spectra), dual oxidation (III/V) states of adsorbed arsenic were observed with As(V) being more noticeable than As(III). This indicates that most of the As(III) got oxidized to As(V) as they reacted with the surface iron oxide layer of the iron nanoparticles present in GNZVI. The adsorption and oxidation of As(III) on the GNZVI surface happened simultaneously. The deconvolution of O1s spectrum of arsenic-sorbed GNZVI show reduction in surface bound –OH concentration in case of As(V) (Fig 7a) and increase in concentration for As(III) (Fig. 7b) compared to pristine GNZVI. This reveals that arsenic species reacted with surface bound oxide and hydroxide of the iron nanoparticles present in GNZVI and formed inner-sphere arsenic-iron complex. Similar observations were recorded by others for iron nanoparticle and arsenic reaction. (Das et al., 2020; Kanel et al., 2006; Wang et al., 2014a; Tucek et al., 2017). For As(V)-sorbed GM, the characteristic peak of As(V) is present at ~ 45.67 eV (Fig. 7c, As3d spectra) confirming the adsorption of As(V) onto the GM surface, and the oxidation state remained unchanged. In case of As(III)-sorbed GM (Fig. 7d, As3d spectra), both As(III) and As(V) peaks can be seen with As(III) being more noticeable than As(V). This indicate most of the sorbed As(III) did not get oxidized but only a smaller fraction was oxidized to As(V). Iron in GM is present in both Fe^{2+} and Fe^{3+} oxidation states, and the surface bound Fe^{2+} induces oxidation of As(III) to As(V) either though Fenton reaction (Liu et al., 2015) or via the formation of Fe(III) oxide-Fe(II)-As(III) surface complexation (Amstaetter et al., 2010; Yan et al., 2012). In O1s spectrum for As(III) and As(V) sorbed GM, the concentration of Fe-O and surface bound hydroxyl changed compared to pristine GM. This also indicates that the arsenic species adsorbed onto surface iron oxide layer via surface complexation.

3.5. Environmental Significance

Both NZVI and magnetite are iron-based nanomaterials which are promoted as promising adsorbents for aqueous arsenic remediation.

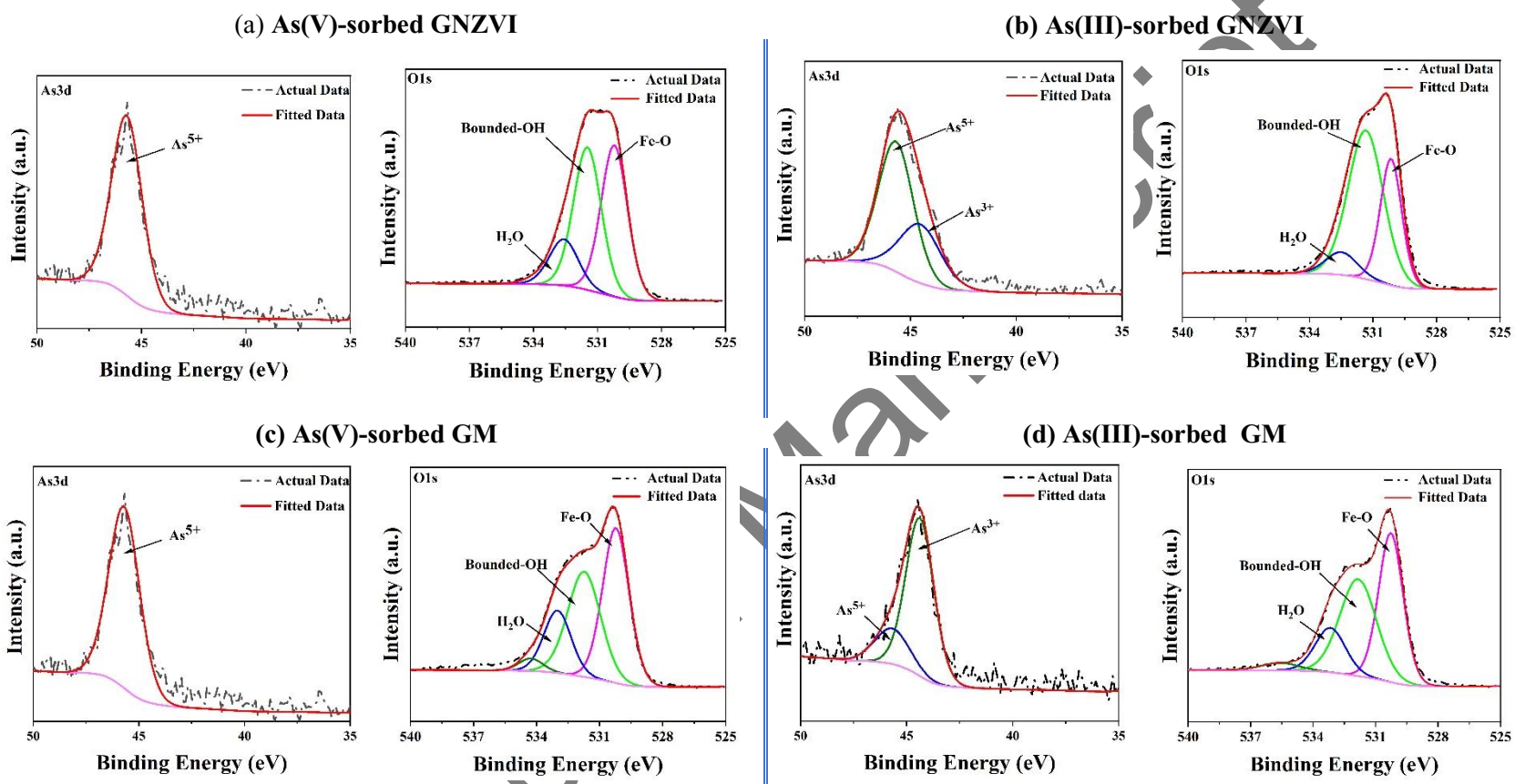

Fig. 7. As3d and O1s XPS spectra for arsenic-sorbed GNZVI and GM. XPS spectra for GNZVI after (a) As(V) sorption, (b) As(III) sorption; and XPS spectra for GM after (c) As(V) sorption, (d) As(III) sorption.

However, one of the major important aspects of its applicability is their efficiency in real water environments which is overlooked by many. Arsenic is predominately present in As(V) oxidation state and our results suggest that magnetite-based nanomaterials work most efficiently (>90%) at pH blow 4 for As(V) removal. So, at typical groundwater pH (6.5-8.5), M based materials cannot potentially perform to its full potential unless pH adjustment is made or an increased adsorbent dosing is added at addition cost to the treatment process. On the contrary, NZVI-based nanomaterials worked equally effective at all environmentally relevant pH (3-9). Besides, arsenic removed per unit mass of Fe present in NZVI-based nanomaterials is much better than in M-based nanomaterials. NZVI-based materials, specifically the GNZVI, hold promise for field applications for the treatment of groundwater contaminated with either or both As(III) and As(V). While M-based nanomaterials may not be effectively and easily used to treat groundwater (pH 6.5-8.5), it may find applications in industrial wastewater or mining drainage water arsenic treatment where solution pH is very low. Manufacturing of iron nanomaterials is an energy and cost intensive process compared to bulk iron based adsorptive media. While iron nanomaterials are far more efficient and effective and required in less amount, the major roadblock for their actual application is their high production cost. In this study, the synthesized GNZVI has exhibited better iron use efficiency (i.e., amount of arsenic removed per unit mass of Fe) and that is expected to lead to cost saving in terms of materials needed and the size of treatment units. This will make the GNZVI-based water treatment systems very sustainable and efficient.

However, one of the major important aspects of its applicability is their efficiency in real water environments which is overlooked by many. Arsenic is predominately present in As(V) oxidation state and our results suggest that magnetite-based nanomaterials work most efficiently (>90%) at pH blow 4 for As(V) removal. So, at typical groundwater pH (6.5-8.5), M based materials cannot potentially perform to its full potential unless pH adjustment is made or an increased adsorbent dosing is added at addition cost to the treatment process. On the contrary, NZVI-based nanomaterials worked equally effective at all environmentally relevant pH (3-9). Besides, arsenic removed per unit mass of Fe present in NZVI-based nanomaterials is much better than in M-based nanomaterials. NZVI-based materials, specifically the GNZVI, hold promise for field applications for the treatment of groundwater contaminated with either or both As(III) and As(V). While M-based nanomaterials may not be effectively and easily used to treat groundwater (pH 6.5-8.5), it may find applications in industrial wastewater or mining drainage water arsenic treatment where solution pH is very low. Manufacturing of iron nanomaterials is an energy and cost intensive process compared to bulk iron based adsorptive media. While iron nanomaterials are far more efficient and effective and required in less amount, the major roadblock for their actual application is their high production cost. In this study, the synthesized GNZVI has exhibited better iron use efficiency (i.e., amount of arsenic removed per unit mass of Fe) and that is expected to lead to cost saving in terms of materials needed and the size of treatment units. This will make the GNZVI-based water treatment systems very sustainable and efficient.

4. Conclusions

This study has, for the first time, compared four frequently reported iron-based nanomaterials for arsenic removal under the same experimental conditions, and selected the best candidate for potential field application to remove arsenic from water. The nanoscale zero-valent iron (NZVI)-based material showed better removal performance over a wide range of pH (3-9) for both As(III) and As(V). The authors explored the potential mechanisms of arsenic removal by NZVI-based nanomaterials and opined that arsenic removal was controlled by electrostatic forces and surface complexation. The magnetite (M)-based nanomaterials worked better (>90%) at low pH (pH < 4) only for As(V) with the removal being controlled by electrostatic interactions. On the other hand, As(III) removal by M-based nanomaterials increased with increase in pH as the process was controlled by ligand exchange and surface complexation. The deposition of nanoparticles on GO surface (to form nanohybrids) improved arsenic removal significantly in both the nanohybrids (GNZVI and GM) compared to their base counterparts (NZVI and M), and this happened because of better dispersion of iron nanoparticles on GO surface providing better interaction between arsenic species and nanomaterial reactive surfaces.

GNZVI nanohybrids were found to be the most efficient in terms of arsenic removal per unit mass of iron used and the authors would promote GNZVI as a potential candidate for future field application to remove arsenic from groundwater. It is, however, important to recognize that nano-based adsorbents with high arsenic adsorption capacity always pose a concern for secondary contamination through the release (desorption) of arsenic from the adsorbed phase, and so experiments should be conducted on the long-term stability of arsenic in arsenic saturated nanomaterials with actual groundwater.

Declaration of competing interest

The authors declare that they have no known competing financial interests or personal relationships that could have appeared to influence the work reported in this paper.

Acknowledgments

This work was funded by National Science Foundation (NSF Grant# CBET-1707093), USGS-North Dakota Water Resources Research Institute and North Dakota State University (Grand Challenges Initiative). Tonoy Das received funding through NS-ICAR-IF from Indian Council of Agriculture Research. Electron microscopy was done at the NDSU Core Laboratory (NSF Grant# CMMI-0821655).

References

Amini M, Abbaspour KC, Berg M, Winkel L, Hug SJ, Hoehn E, et al. Statistical modeling of global geogenic arsenic contamination in groundwater. Environmental Science & Technology 2008; 42: 3669-3675.

Amstaetter K, Borch T, Larese-Casanova P, Kappler A. Redox Transformation of Arsenic by Fe(II)-Activated Goethite (alpha-FeOOH). Environmental Science & Technology 2010; 44: 102-108.

Andjelkovic I, Tran DNH, Kabiri S, Azari S, Markovic M, Losic D. Graphene Aerogels Decorated with alpha-FeOOH Nanoparticles for Efficient Adsorption of Arsenic from Contaminated Waters. ACS Applied Materials & Interfaces 2015; 7: 9758-9766.

Agency for Toxic Substances and Disease Registry (ATSDR). Toxicological profile for arsenic. Agency for Toxic Substances and Disease Registry, Division of Toxicology, Atlanta, GA 2007.

Balistrieri LS, Murray JW. The surface-chemistry of goethite (alpha-FeOOH) in major ion seawater. American Journal of Science 1981; 281: 788-806.

Ben Issa N, Rajakovic-Ognjanovic VN, Marinkovic AD, Rajakovic LV. Separation and determination of arsenic species in water by selective exchange and hybrid resins. Analytica Chimica Acta 2011; 706: 191-198.

Bezbaruah AN, Kalita H, Almeelbi T, Capecchi CL, Jacob DL, Ugrinov AG, et al. Ca-alginate-entrapped nanoscale iron: arsenic treatability and mechanism studies. Journal of Nanoparticle Research 2013; 16.

Chandra V, Park J, Chun Y, Lee JW, Hwang I-C, Kim KS. Water-Dispersible Magnetite-Reduced Graphene Oxide Composites for Arsenic Removal. ACS Nano 2010; 4: 3979-3986.

Chen ML, Sun Y, Huo CB, Liu C, Wang JH. Akaganeite decorated graphene oxide composite for arsenic adsorption/removal and its proconcentration at ultra-trace level. Chemosphere 2015; 130: 52-58.

Das TK, Sakthivel TS, Jeyaranjan A, Seal S, Bezbaruah AN. Ultra-high arsenic adsorption by graphene oxide iron nanohybrid: Removal mechanisms and potential applications. Chemosphere 2020; 253.

Gao W. The chemistry of graphene oxide. Graphene oxide. Springer, 2015, pp. 61-95.

Grosvenor AP, Kobe BA, Biesinger MC, McIntyre NS. Investigation of multiplet splitting of Fe 2p XPS spectra and bonding in iron compounds. Surface and Interface Analysis 2004; 36: 1564-1574.

Hoan NTV, Thu NTA, Van Duc H, Cuong ND, Khieu DQ, Vo V. Fe_3O_4/Reduced Graphene Oxide Nanocomposite: Synthesis and Its Application for Toxic Metal Ion Removal. Journal of Chemistry 2016: 10.

International Organization for Standardization (ISO), ISO BS 14887 (2000) Sample preparation-dispersing procedures for powders in liquids, International Organization for Standardization, Geneva, Switzerland (2000).

Kanel SR, Greneche J-M, Choi H. Arsenic (V) removal from groundwater using nano scale zero-valent iron as a colloidal reactive barrier material. Environmental science & technology 2006; 40: 2045-2050.

Krajangpan S, Kalita H, Chisholm BJ, Bezbaruah AN. Iron Nanoparticles Coated with Amphiphilic Polysiloxane Graft Copolymers: Dispersibility and Contaminant Treatability. Environmental Science & Technology 2012; 46: 10130-10136.

Kumar ASK, Jiang SJ. Synthesis of magnetically separable and recyclable magnetic nanoparticles decorated with beta-cyclodextrin functionalized graphene oxide an excellent adsorption of As(V)/(III). Journal of Molecular Liquids 2017; 237: 387-401.

Lata S, Samadder SR. Removal of arsenic from water using nano adsorbents and challenges: A review. Journal of Environmental Management 2016; 166: 387-406.

Lataye DH, Mishra IM, Mall ID. Removal of pyridine from aqueous solution by adsorption on bagasse fly ash.

Industrial & Engineering Chemistry Research 2006; 45: 3934-3943.

Liu CH, Chuang YH, Chen TY, Tian Y, Li H, Wang MK, et al. Mechanism of Arsenic Adsorption on Magnetite Nanoparticles from Water: Thermodynamic and Spectroscopic Studies. Environmental Science & Technology 2015; 49: 7726-7734.

Liu J, Jiang J, Meng Y, Aihemaiti A, Xu Y, Xiang H, et al. Preparation, environmental application and prospect of biochar-supported metal nanoparticles: A review. Journal of Hazardous Materials 2020: 122026.

Martin JE, Herzing AA, Yan WL, Li XQ, Koel BE, Kiely CJ, et al. Determination of the oxide layer thickness in core-shell zerovalent iron nanoparticles. Langmuir 2008; 24: 4329-4334.

Mishra AK, Ramaprabhu S. Ultrahigh arsenic sorption using iron oxide-graphene nanocomposite supercapacitor assembly. Journal of Applied Physics 2012; 112.

Morin G, Wang YH, Ona-Nguema G, Juillot F, Calas G, Menguy N, et al. EXAFS and HRTEM Evidence for As(III)-Containing Surface Precipitates on Nanocrystalline Magnetite: Implications for As Sequestration. Langmuir 2009; 25: 9119-9128.

Murcott S. Arsenic contamination in the world: IWA publishing, 2012.

Podgorski J, Berg M. Global threat of arsenic in groundwater. Science 2020; 368: 845-850.

Rashid US, Saini-Eidukat B, Bezbaruah AN. Modeling arsenic removal by nanoscale zero-valent iron. Environmental Monitoring and Assessment 2020; 192.

Sheng GD, Li YM, Yang X, Ren XM, Yang ST, Hu J, et al. Efficient removal of arsenate by versatile magnetic graphene oxide composites. RSC Advances 2012; 2: 12400-12407.

Sherlala AIA, Raman AAA, Bello MM, Asghar A. A review of the applications of organo-functionalized magnetic graphene oxide nanocomposites for heavy metal adsorption. Chemosphere 2018; 193: 1004-1017.

Siddiqui SI, Naushad M, Chaudhry SA. Promising prospects of nanomaterials for arsenic water remediation: A comprehensive review. Process Safety and Environmental Protection 2019; 126: 60-97.

Su H, Ye ZB, Hmidi N. High-performance iron oxide-graphene oxide nanocomposite adsorbents for arsenic removal. Colloids and Surfaces a-Physicochemical and Engineering Aspects 2017; 522: 161-172.

Tucek J, Prucek R, Kolarik J, Zoppellaro G, Petr M, Filip J, et al. Zero-Valent Iron Nanoparticles Reduce Arsenites and Arsenates to As(0) Firmly Embedded in Core-Shell Superstructure: Challenging Strategy of Arsenic Treatment under Anoxic Conditions. ACS Sustainable Chemistry & Engineering 2017; 5: 3027-3038.

United States Environmental Protection Agency (USEPA). National primary drinking water regulations; arsenic and clarifications to compliance and new source contaminants monitoring. Fed Reg 2001; 66: 6975-7066.

Wang C, Luo HJ, Zhang ZL, Wu Y, Zhang J, Chen SW. Removal of As(III) and As(V) from aqueous solutions using nanoscale zero valent iron-reduced graphite oxide modified composites. Journal of Hazardous Materials 2014a; 268: 124-131.

Wang YH, Morin G, Ona-Nguema G, Brown GE. Arsenic(III) and Arsenic(V) Speciation during Transformation of Lepidocrocite to Magnetite. Environmental Science & Technology 2014b; 48: 14282-14290.

World Health Organization (WHO). Arsenic in drinking-water: background document for development of WHO guidelines for drinking-water quality. World Health Organization, 2003.

World Health Organization (WHO). Arsenic Fact Sheet, 2018, Available at: https://www.who.int/news-room/fact-sheets/detail/arsenic. (Access March 23, 2020).

Wong WW, Wong HY, Badruzzaman ABM, Goh HH, Zaman M. Recent advances in exploitation of nanomaterial for arsenic removal from water: a review. Nanotechnology 2017; 28.

Wu C, Tu JW, Liu WZ, Zhang J, Chu SQ, Lu GN, et al. The double influence mechanism of pH on arsenic removal by nano zero valent iron: electrostatic interactions and the corrosion of Fe-0. Environmental Science-Nano 2017; 4: 1544-1552.

Yan WL, Ramos MAV, Koel BE, Zhang WX. As(III) Sequestration by Iron Nanoparticles: Study of Solid-Phase Redox Transformations with X-ray Photoelectron Spectroscopy. Journal of Physical Chemistry C 2012; 116: 5303-5311.

Yang X, Xia L, Song S. Arsenic adsorption from water using graphene-based materials as adsorbents: A critical review. Surface Review and Letters 2017; 24.

Yoon Y, Park WK, Hwang TM, Yoon DH, Yang WS, Kang JW. Comparative evaluation of magnetite-graphene oxide and magnetite-reduced graphene oxide composite for As(III) and As(V) removal. Journal of Hazardous Materials 2016; 304: 196-204.

Yoon Y, Zheng M, Ahn YT, Park WK, Yang WS, Kang JW. Synthesis of magnetite/non-oxidative graphene composites and their application for arsenic removal. Separation and Purification Technology 2017; 178: 40-48.

Yu XW, Wei YF, Liu CB, Ma JH, Liu H, Wei SD, Deng W, Xiang J, Luo S. Ultrafast and deep removal of arsenic in high-concentration wastewater: A superior bulk adsorbent of porous Fe_2O_3 nanocubes-impregnated graphene aerogel. Chemosphere 2019; 222: 258-2